Advanced Steel Construction – Vol. 21 No. 1 (2025) 54–63
DOI:10.18057/IJASC.2025.21.1.5

BENDING CAPACITY OF COLD-FORMED THIN-WALLED STEEL TUBES INFILLED WITH GYPSUM

Bo Su [1,*], Yi-Wen Liu [1] and Jiao Zhang [2]

[1] *Department of Civil Engineering, Jiangsu University, Zhenjiang, 212000, China*
[2] *School of Building Engineering, Changzhou Vocational Institute of Engineering, Changzhou, 213161, China*
** (Corresponding author: E-mail: subo@ujs.edu.cn)*

ABSTRACT

Cold-formed thin-walled steel tubes (CTSP) find common use in light steel structures and solar panel brackets, yet they are prone to collapse due to local instability and bending failure. To enhance the bending capacity of CTSP, this paper introduces a new composite structure known as gypsum-reinforced cold-formed thin-walled steel tubes (GCTSP), aiming to preserve high stiffness, stability, and lightweight characteristics. The study proceeds in two main phases: Three types of GCTSP (Section sizes of 80mm×40mm, 80m×60mm, 80mm×80mm) undergo four-point bending experiments to determine components' ultimate bending capacity. Finite element (FE) models are established to investigate the influence of different aspect ratios (1.00, 1.14, 1.33, 1.60, 2.00) on the bending capacity of GCTSP. Gypsum has been shown to significantly improve the bending capacity of CTSP. This study emphasizes considerable impact of changes in aspect ratio on GCTSP, leading to an increase in bearing capacity between 22% and 90%. Additionally, a proposed calculation formula, accounting for both gypsum reinforcement and aspect ratio effects, demonstrates excellent alignment with experimental data, yielding an error rate below 4%. This study provides valuable insights for enhancing the flexural bearing capacity of GCTSP through gypsum reinforcement, considering different aspect ratios.

ARTICLE HISTORY

Received: 4 March 2024
Revised: 6 December 2024
Accepted: 7 December 2024

KEYWORDS

CTSP;
Gypsum;
Four-point bending;
Composite structure;
Finite Element

1. Introduction

CTSP provide benefits including light weight, high strength, ease of prefabrication, fast assembly, and recyclability. Their widespread use in steel structure housing, factory buildings, sunrooms, and various engineering projects and auxiliary structures has significantly contributed to the development of lightweight assembled green buildings, showcasing broad application prospects [1]. However, the inherent challenge of these tubes lies in their thin wall with small thickness (1.5 mm-3.0 mm), resulting in issues such as low stiffness and poor stability. These limitations restrict their spanning and bearing capacities. In the face of strong wind loads, earthquakes, or snowstorms, these structures may be susceptible to collapse due to local instability and bending failure of components, leading to substantial property losses and potential casualties [2-4].

Researchers have thoroughly studied the mechanical properties of CTSP. For instance, Yongbo Shao et al. [7] carried out a finite element analysis to investigate the axial behavior of square steel tubes. Their calculations revealed that the buckling coefficient closely resembles that of a simply supported thin plate under axial compression, providing a valuable reference for the stability calculation of square steel tubes. Paola Pannuzzo et al. [8] explored the bending behavior of square and rectangular hollow CTSP after heat treatment through three-point bending tests and numerical simulation studies. Noteworthy references, such as the European standard [9] and AISC 360-16 [10], have categorized cold-formed steel into different cross-sections and provided calculation methods for the flexural ultimate of CTSP. More recently, Melina Bosco et al. [11] have developed and studied formulas that consider parameters such as slenderness ratio, shear length, and axial load. CTSP clearly show limitations in both overall and local stability, as well as bending capacity, which undermine structural reliability.

To enhance the bearing capacity of rectangular steel tubes, various studies have explored the use of CFSTs and their mechanical capabilities. Lin Xiao et al. [12] conducted a comprehensive review of the current research on concrete-filled steel tubes in bridge structures. They highlighted potential areas for future research, including bending capacity, spatial stress characteristics, dynamic response, and local stress characteristics. Zijian Chen et al. [13] concentrated on the axial compression capacity of steel-reinforced concrete short columns, consolidating design formulas, material constitutive models, and experimental research conclusions from various countries. This work provides a valuable reference for further investigations into the axial compression capacity of steel-reinforced concrete. Saifeng Wu et al. [14] developed CFSTs that inherit the advantages of traditional reinforced concrete columns and have been utilized in several super high-rise buildings. However, it is worth noting that current scholarly attention is predominantly focused on the research of CFSTs, with limited studies on the flexural capacity of steel tubes.

In addition to concrete, researchers have explored the use of lighter materials, such as gypsum, to form composite thin-walled steel components. For instance, Yifeng Xu [15] proposed and studied phosphogypsum-filled thin-walled square steel short columns. Filling phosphogypsum into thin-walled square steel tubes not only enhances their compressive capacity but also preserves their "lightweight" characteristics. Yuan et al. [16] introduced a composite steel tube filled with gypsum slurry and waste concrete blocks. This tube exhibits early strength, fast hardening, and high bearing capacity, making it suitable for use as temporary components in the construction of emergency rescue and disaster relief houses. However, while the mentioned contributions focus on the compressive capacities of gypsum-filled columns, there is still a gap in research regarding the bending capacity of gypsum-filled beams.

This study aims to analyze the bending capacity of GCTSP. Section 2 outlines the experimental programs, including material preparation, test cases, and device installation. Section 3 provides an in-depth analysis of the test results. Section 4, numerical models are established for simulation, and the analysis of the aspect ratio effect on mechanical capacity is presented. Section 5 introduces a practical theoretical formula for calculating the flexural capacity, taking into account the plastic development coefficient. While scholars have started to recognize the lightweight and high-strength characteristics of steel tubes filled with gypsum, research on gypsum-filled steel tubes remains limited, particularly in terms of their bending capacity.

2. Experimental program

2.1. Materials preparation: steel tubes and gypsum

The gypsum manufacturer is produced by Shandong Taiyuan Gypsum Technology Co., Ltd. As the setting final setting time of pure gypsum is too short for specimen preparation, a 0.12 % dosage of retarder is added to prong its final setting time (135 minutes). The retarder is wheat protein hydrolysate provided by Beijing Longtengda Chemical Co., Ltd. Table 1 presents properties of gypsum.

Table 1
Physical properties of gypsum

Name	Initial setting time/min	Final setting time/min	Break off strength/MPa	Compressive strength/MPa	Measurement of powders/%	Whiteness/%
Gypsum	5	10	3.5	16	0.01	50

The hollow galvanized square steel tubes are manufactured by Tianjin Steel Co., Ltd. It is made of Q235 grade steel mechanical properties illustrates in Table 2.

Table 2
Material properties of Q235

Name	Density g/cm^3	Tensile strength/Mpa	Yield strength/ MPa	Elongation	Impact ductility /J	Welding property
Q235 steel tube	7.85	370-500	235	> 25%	27-30	better

2.2. Test cases

As depicted in Table 3, each cross-sectional steel tube undergoes two working conditions (hollow or fully filled by gypsum), and each working condition includes two similar members to obtain average test results. In total, 12 members are tested in this study. Q235, being a commonly used model in engineering, was chosen for its combination of lightweight and high strength. As a result of this property, the CTSP with a smaller cross-sectional size was selected to investigate its bending characteristics. The dimensions of three types of Q235 CTSP are illustrated in Fig. 1.

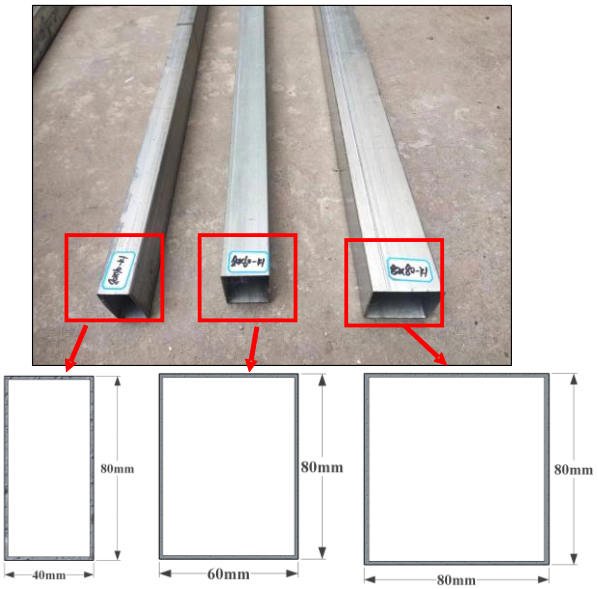

Fig. 1 Cold-formed thin-walled steel tubes and their section size

Table 3
Test cases

No.	Test condition	Cross section	Aspect ratio	Gypsum filling
1	80×40-k	80mm×40mm	2	Yes
2	80×40-s			No
3	80×60-k	80mm×60mm	1.33	No
4	80×60-s			yes
5	80×80-k	80mm×80mm	1	No
6	80×80-s			yes

Note: k indicates that the steel tube is hollow, and s indicates that the steel tube is full filled with gypsum.

2.3. Test procedures

2.3.1. Preparation of GCTSP specimens

The CTSP has a length of 1500 mm and a thickness of 1.5 mm. To examine the impact of aspect ratio on the filling effect, three cross-sectional types are selected (80 mm × 40 mm, 80 mm × 60 mm, and 80 mm × 80 mm). After weighing a certain quantity of gypsum, water, and retarder, mix them into a uniform slurry, as shown in Fig. 2(a). Finally, pour the mixed gypsum slurry into the empty tube using a funnel until the compactness is 100%, as depicted in Fig. 2(b). A one-week maintenance period is required for the gypsum to achieve the maximum strength standard when poured into the three types of steel tubes, as illustrated in Fig. 2 (c), for the three types of GCTSP sections with a filling rate of 100%.

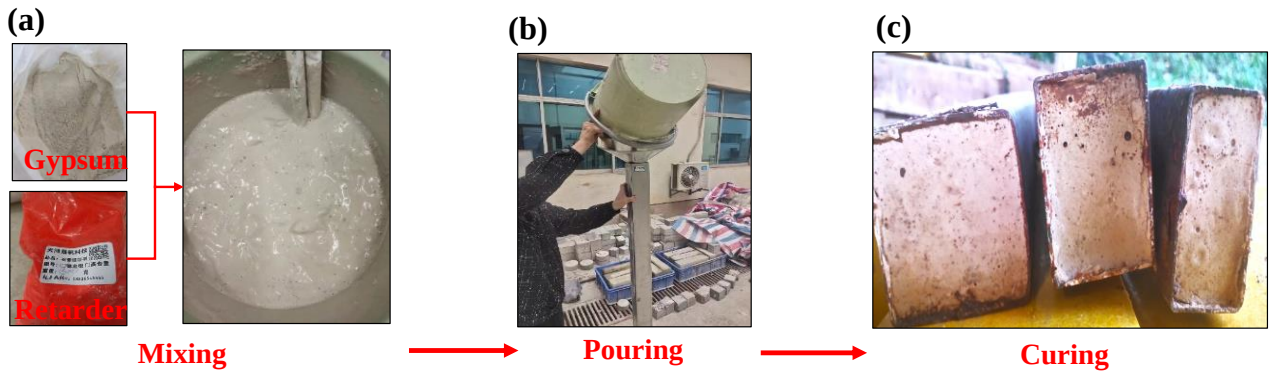

Fig. 2 The preparation process of GCTSP: (a) Mixing gypsum and retarder; (b) Pouring gypsum slurry; (b) Curing specimens

2.3.2. Strain gauges

In Fig. 3, To monitor strain distribution, seven sensors are placed at the central section of the specimen, with five (No. 1 to No. 5) arranged vertically along its height. Additionally, two strain gauges (No.6 and No.7) are positioned at the middle points of the top and bottom surfaces to measure tensile and compressive strains on the surface.

2.3.3. Test loading

The four-point bending tests are conducted in the Civil Engineering Laboratory of Jiangsu University. As illustrated in Fig. 4, the test system comprises a 50T self-balanced structure vertical loading reaction system with a separated hydraulic jack, simple supports at both ends, a universal compression hinge, a pressure sensor, and strain and displacement gauges. Prior to the four-point bending test, adjustments are made to the distribution beam, loading hinge point distance, and bearing position in the vertical loading reaction system of the self-balanced structure.

After installing both the hollow and gypsum-reinforced cold-formed thin-walled steel tubes, three displacement meters (dial indicators) are set up using magnetic supports to record the specimen's displacement at midspan and two ends [18]. The vertical force of the hydraulic jacks is distributed by the distribution beam to two concentrated loads at the steel rollers with a distance of 400 mm. Before the formal loading, a preload force with a value of 0.5kN is applied to ensure that the loading rollers are in full contact with the specimen. Subsequently, the load is unloaded to zero, and then continuously increased with a step of 0.5kN until the tube is destroyed.

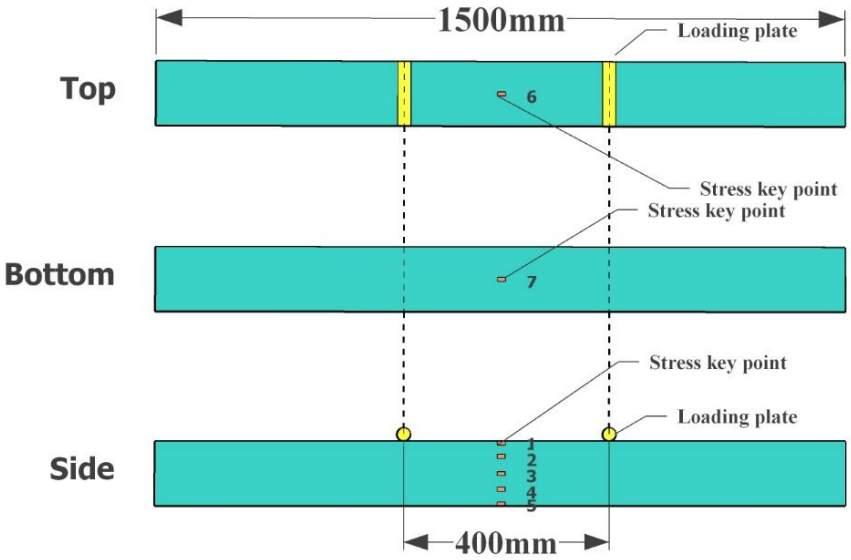

Fig. 3 Arrangement of strain gauges at midspan section

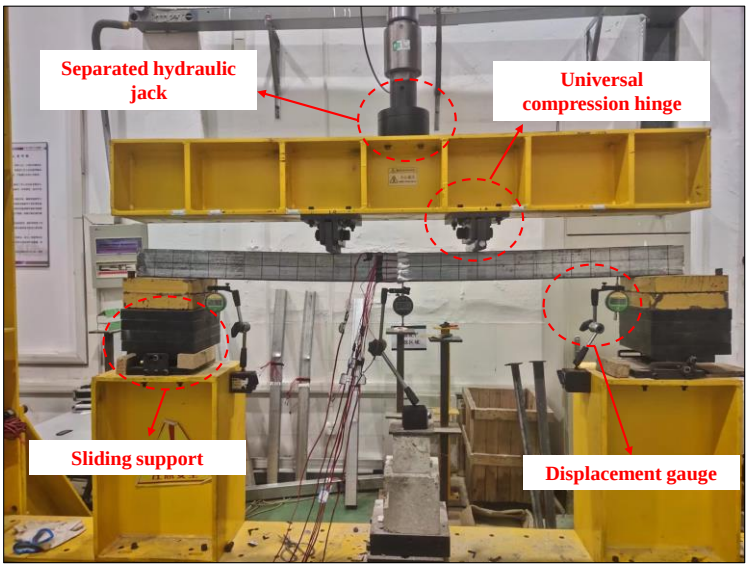

Fig. 4 50T self-balancing vertical loading reaction system

3. Test results and discussion

3.1. Load–deflection behavior

At the beginning of the four-point bending tests, the entire component undergoes slight bending deformation without any significant local changes. Nevertheless, with the increase in loading value, the steel plate at loading point slowly depresses, resulting in noticeable bulging protrusions on the front and back sides of the steel tube. Finally, complete buckling failure occurs around the loading points, leading to the component reaching its ultimate load capacity. However, the failure patterns exhibit variations with changes in aspect ratios. As illustrated in Fig. 5(a), local buckling in the 80×40-k tube is more pronounced and localized, effectively highlighting the stress concentration phenomenon. The degree of local failure of the 80×60-k and 80×80-k tubes is less than that of the 80×40-k tube; however, it appears that local buckling expands along the horizontal direction to a larger area (Fig. 5(b)-Fig. 5(c)).

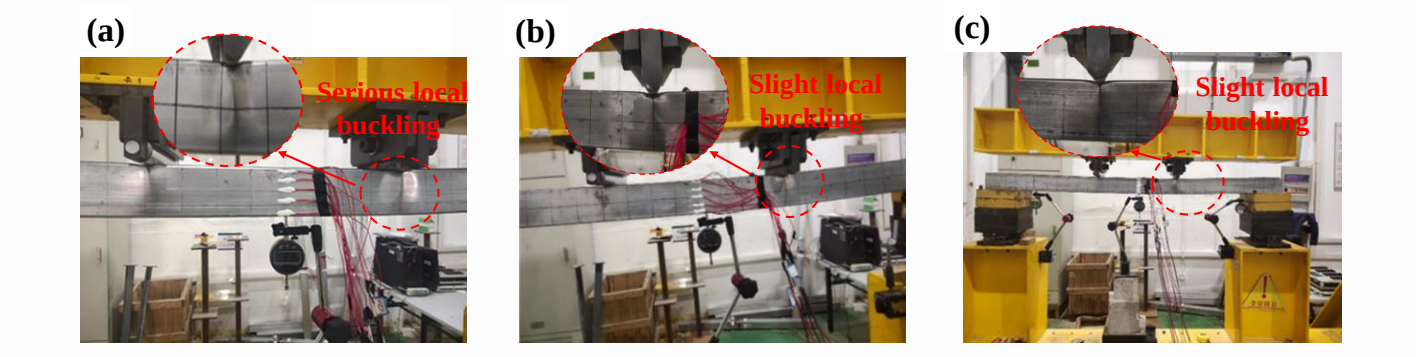

Fig. 5 Failure mode of the hollow steel tubes. (a) 80×40-k; (b) 80×60-k; (c) 80×80-k

During the four-point bending tests on GCTSP, none of the three types of specimens (80×40-s, 80×60-s, 80×80-s) produced noticeable sounds and maintained load-bearing capacity until local buckling occurred at the midspan. However, when compared with the corresponding hollow tubes, GCTSP exhibited smaller localized deformation areas and reduced the crushing degree of the upper surface at the loading points. Evidently, the infilled gypsum provides support to the steel tubes, alleviating stress concentration and enhancing overall bending capacity (Fig. 6(a)-Fig. 6(c)). However, due to the smallest aspect ratio (1.0) of the 80×80-s steel tube, the constraint effect between gypsum and steel panels is less than that of the 80×40-s and 80×60-s tubes. As seen in Fig. 6(c), two local buckling zones occur symmetrically along 45° angles below the loading points, indicating the shearing failure of the inner gypsum.

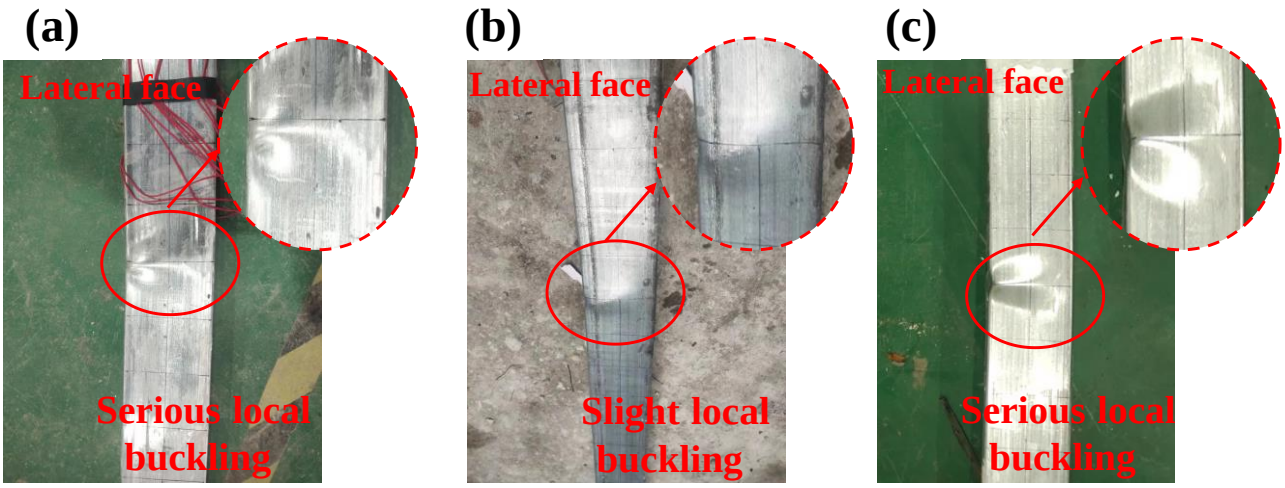

Fig. 6 local failure of different GCTSP. (a) 80×40-s; (b) 80×60-s; (c) 80×80-s

3.2. Flexural Capacity of Gypsum-Reinforced Steel Tubes

3.2.1. The improvement of bending bearing capacity

The load-deflection curves of both the hollow and gypsum-infused steel tubes are illustrated in Fig. 7. In Fig. 7(a), for the steel tubes with a section size of 80mm×40mm, the curves for both hollow and infused tubes are initially linear and nearly coincident. However, as the loading process progresses, the slope of the curve (representing bending stiffness) for the hollow tubes decreases abruptly, reaching its ultimate load value quickly. In contrast, the infused tubes exhibit significantly larger plastic deformation and better load-bearing capacity.

Moving to Fig. 7(b), which represents steel tubes with a section size of 80 mm × 60 mm, the slope of the curve for the infused tubes is consistently larger than that of the hollow tubes throughout the loading process, indicating superior load-bearing capacity. Finally, in Fig. 7(c) for steel tubes with a section size of 80 mm × 80 mm, the stiffness and load-bearing capacity of the infused tubes surpass those of the hollow tubes during the entire loading process. The larger aspect ratio (1.33) of the 80×60-s specimen enhances the constraint effect between the gypsum and steel panels, leading to an improved overall bending capacity.

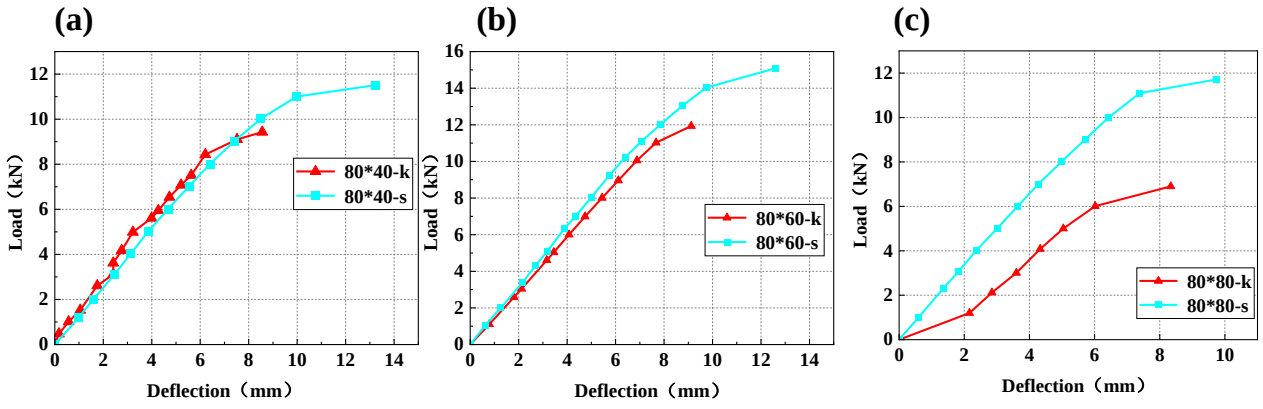

Fig. 7 Load-deflection cures of hollow and gypsum infilled steel tubes

Table 4
Bending capacity of hollow steel tubes

Number	Ultimate bearing capacity /kN	Average value/kN	Number	Ultimate bearing capacity /kN	Average value/ kN	Increased proportion/%
80×40-k1	9.4	9.5	80×40-s1	11.5	11.5	22
80×40-k2	9.5		80×40-s2	11.6		
80×60-k1	11.0	11.5	80×60-s1	15.0	15.1	36
80×60-k2	11.9		80×60-s2	15.1		
80×80-k1	6.9	6.9	80×80-s1	11.1	11.4	90
80×80-k2	6.9		80×80-s2	11.7		

The experimental results, presented in Table 4, show the ultimate bending capacity of both hollow and infilled steel tubes. The ultimate bending capacity of GCTSP for the 80 mm × 40 mm, 80 mm × 60 mm, and 80 mm × 80 mm sections are 11.5 kN, 15.1 kN, and 11.4 kN, respectively, representing increases of 22%, 36%, and 90% compared to the corresponding hollow tubes. It is clear that the aspect ratio plays a crucial role in determining the ultimate load-bearing capacity and plastic deformation characteristics of GCTSP.

3.2.2. Stress-strain at mid span

Fig. 8 shows the variations in load and strain at the mid-section of square steel tubes with different cross-sections. The y-axis shows the applied load, while the x-axis depicts the corresponding axial strain.. Fig. 8(a) illustrates the variation curve for the 80×40-k configuration, and Fig. 8(b) depicts the curve for the 80×40-s configuration. Both configurations demonstrate compliance with the assumption of a flat cross-section. The interaction with gypsum enhances the ductility of the steel tube, thereby increasing its restraint capacity, leading to significant improvements in both maximum load and strain. (Fig. 8(c) and Fig. 8(d)) The variation curves for the 80×60-k and 80×60-s configurations are presented. Here, the influence of aspect ratio is apparent, with the GCTSP performance optimal at this size, exhibiting the best flexural capacity among the three sizes. Local strains of up to 2500με are observed. Lastly, Fig. 8(e) and Fig. 8(f) demonstrate the variation curves for the 80×80-k and 80×80-s configurations, respectively. As the aspect ratio decreases, the steel tube's constraint on the gypsum weakens, reducing the GCTSP's ductility and resulting in smaller maximum strains at the tube's bottom, reaching only 1600 με.

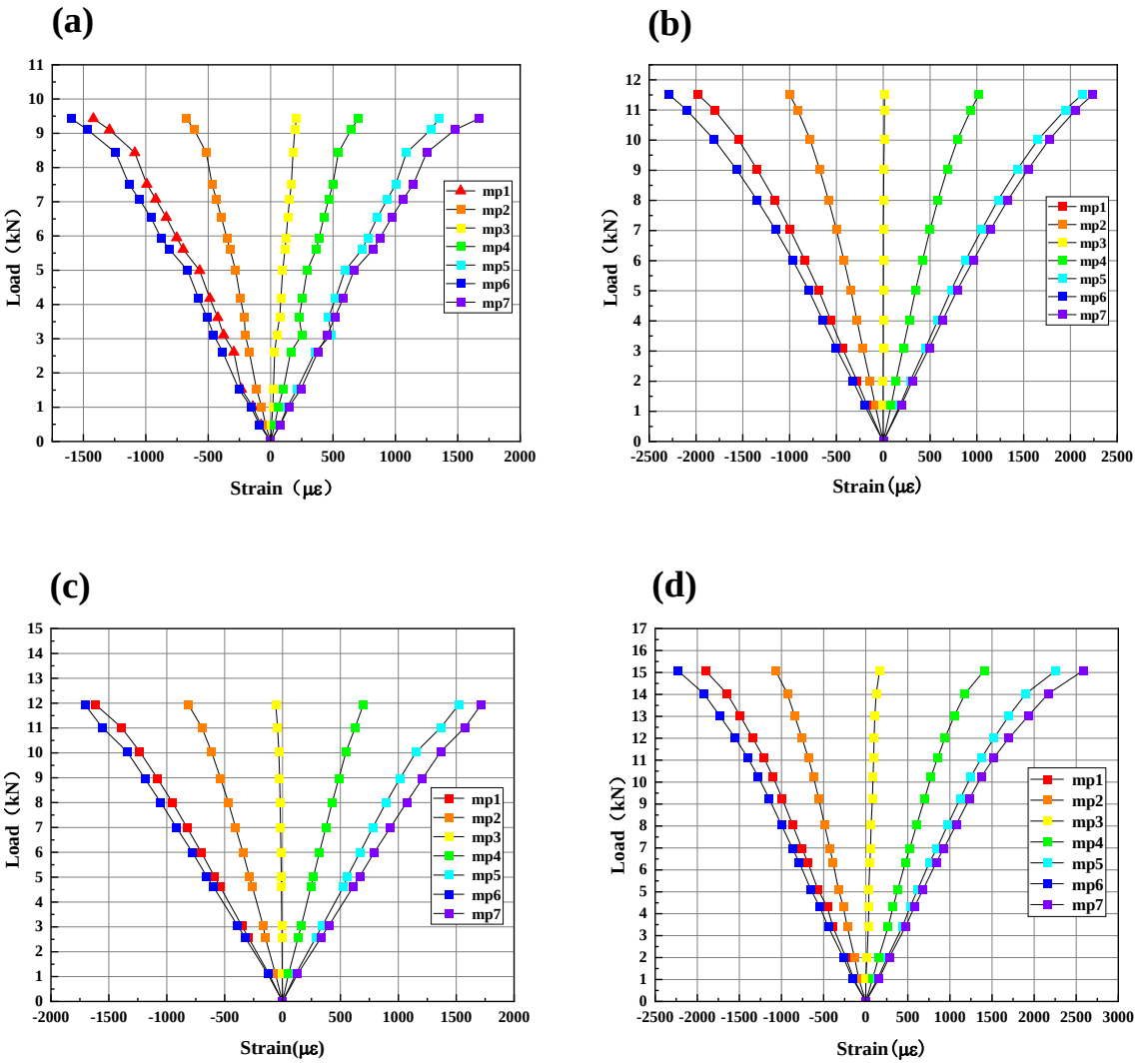

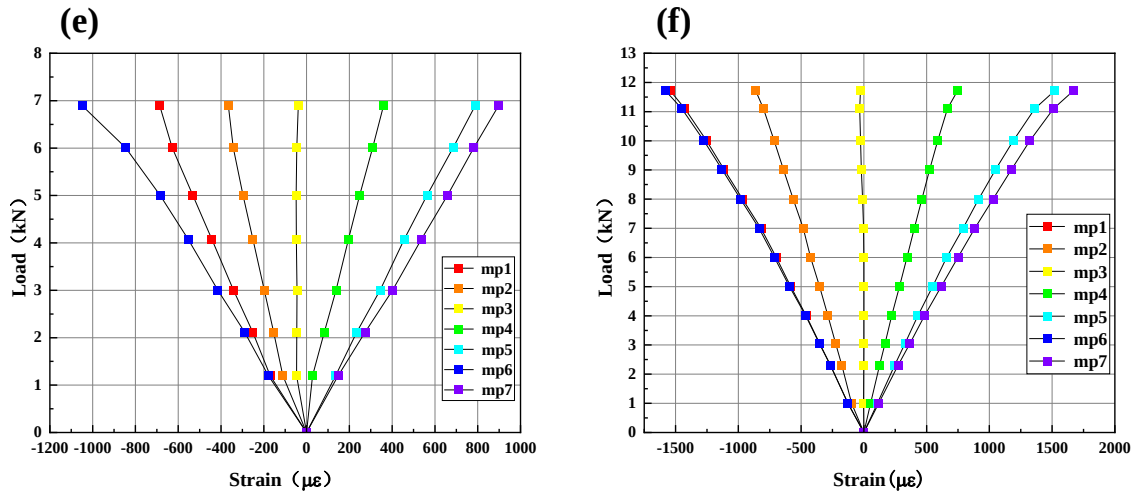

Fig. 8 Stress-strain curves of components with different sizes. (a) 80×40-k; (b)80×40-s; (c) 80×60-k; (d) 80×60-s; (e) 80×80-k; (f) 80×80-s

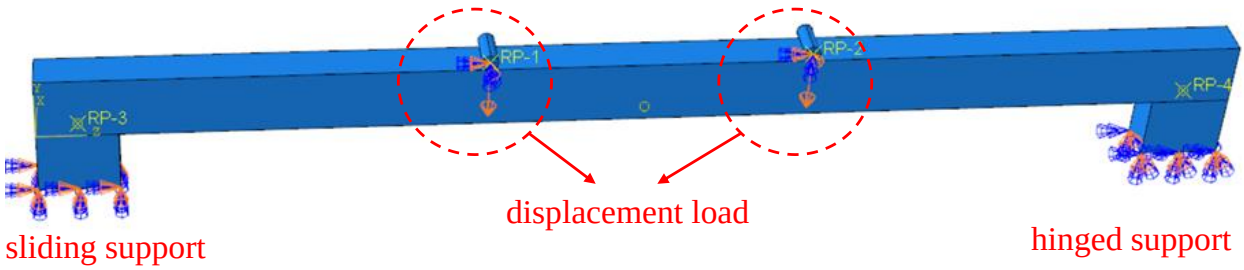

Fig. 9 Boundary conditions of GCTSP

4. Numerical simulation

4.1. FE model

4.1.1. Boundary conditions and grid division

In the experiment, one end of the GCTSP is a hinged support and the other end is a sliding support. The two ends of the component are not limited by the device to limit the displacement on both sides, so the degrees of freedom on both sides are not limited in the simulation. We simplify the 50T self-balancing vertical reaction loading system into two circular loading columns. One loading point has only the degree of freedom of rotation, and the other is completely constrained Fig. 9. The degree of freedom is set as a rigid body, including the pad at the bottom.

GCTSP is modeled using C3D8R linear hexahedral elements and S4R linear quadrilateral elements. This meshing approach reduces computation time while enhancing calculation accuracy. To guarantee the calculation's accuracy [20], it is recommended that the aspect ratio of the element is below 2.0. The model contains a total of 42563 nodes and 36496 elements.

The ' general static ' solver in Abaqus is used to solve the problem of GCTSP material nonlinearity. The loading method is realized by displacement loading. The advantage of this loading method is that the displacement control is used instead of the load application to limit the degree of freedom to eliminate the rigid body displacement to achieve a stable contact relationship.

4.1.2. Materials property

The CTSP in GCTSP adopts the double broken line model Fig. 10, and the standard von mises yield surface and related fluidity laws and anisotropy are used to define the properties of CTSP. The corresponding stress and plastic strain are input in Abaqus. Gypsum [19] is an isotropic material, so the ideal elastic-plastic model Fig. 11 can be used for numerical simulation.

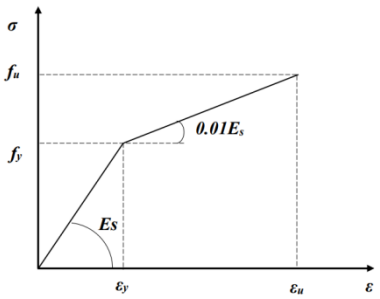

Fig. 10 Steel double broken line model

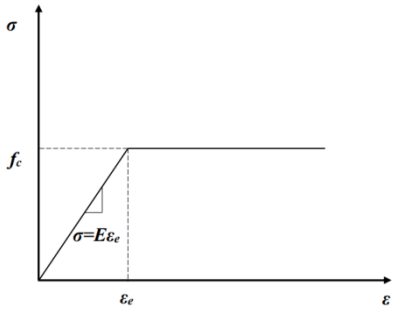

Fig. 11 Ideal elastic-plastic model of gypsum

$$\sigma_s = \begin{cases} E_s\varepsilon_s & ,(\varepsilon \le \varepsilon_y) \\ f_y + \alpha E_s(\varepsilon_s - \varepsilon_y), & (\varepsilon > \varepsilon_y) \end{cases}, \quad (1)$$

where αE_s is the elastic modulus of steel in the strengthening stage, α is 0.01.

$$\sigma_s = \begin{cases} E\varepsilon_e, & (\varepsilon \le \varepsilon_y) \\ f_c & ,(\varepsilon > \varepsilon_y) \end{cases}, \quad (2)$$

where f_c is ultimate compressive strength, ε_e is compressive strain.

4.1.3. Contact interaction

Because there is no device to limit slip in the test, It is essential to account for the effect on bond slip in the numerical simulation. The contact between CTSP and gypsum is defined as surface to surface, and the tangential contact needs to be defined as fiction formulation [20,21]. Penalty, friction coefficient is 0.1, and normal contact is hard contact. The master-slave surface selection assigns the stiffer surface as the master. Thus, the steel tube's internal surface is the master, the gypsum-steel tube contact surface is the slave, and the steel tube is modeled with shell elements. Thus, the steel tube thickness must be considered during setup, with the shell thickness defined to extend 1.5 mm from the bottom to prevent surface penetration.

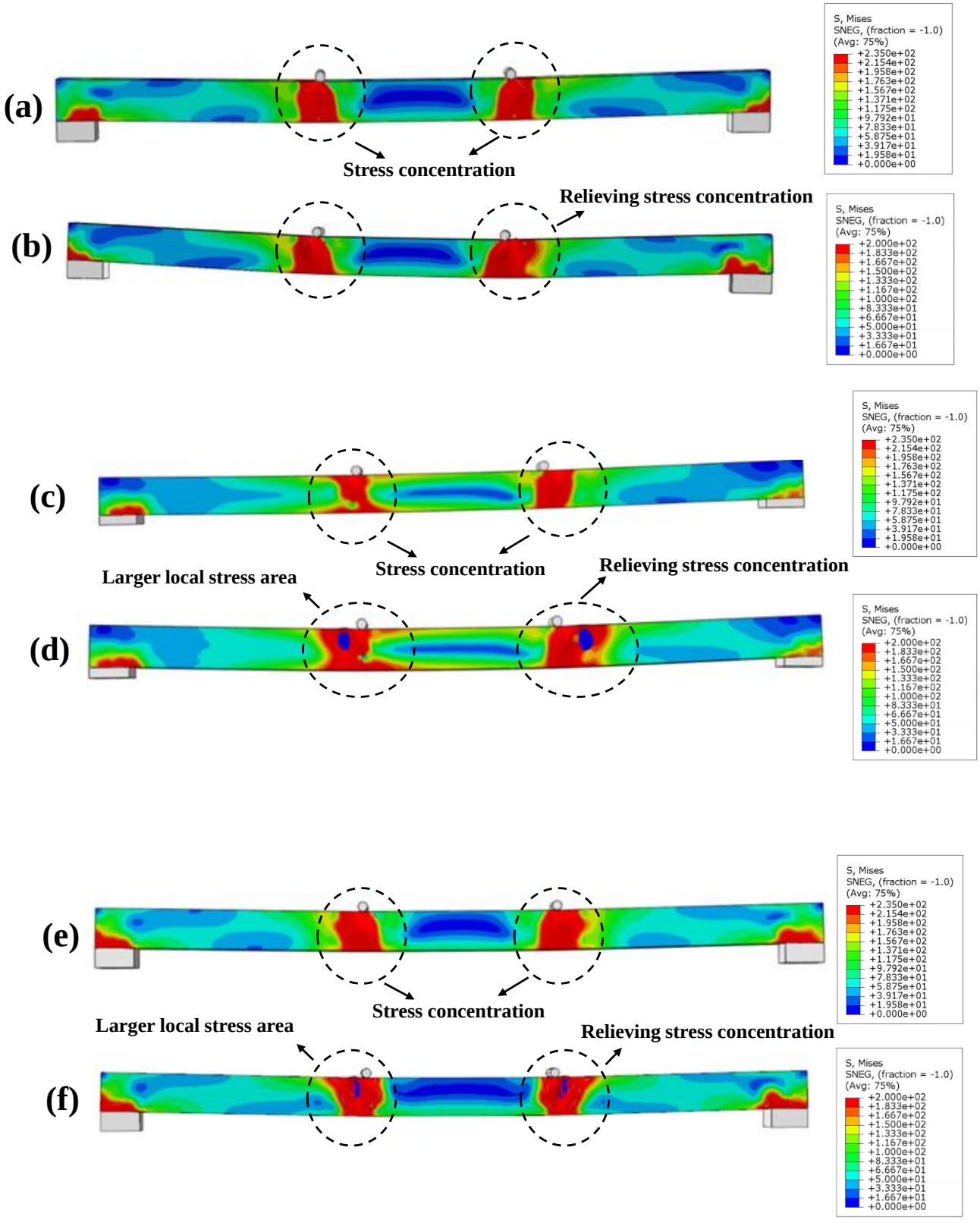

Fig. 12 The stress cloud diagram of different size components. (a) 80×40-k; (b) 80×40-s;(c) 80×60-k; (d) 80×60-s; (e) 80×80-k; (f) 80×80-s

4.2. Result and analysis

4.2.1. Stress cloud

In Fig. 12(a)-(f), the stress-strain diagrams of the gypsum-reinforced cold-formed thin-walled steel tubes with dimensions 80×40-s, 80×60-s, and 80×80-s align with the experimental results. From the stress contour plots in Fig. 12 (a)-(f), it can be observed that the stress distribution aligns with the experimental failure patterns. However, for the hollow steel tube, the stress concentration area at the loading point is relatively small and accompanied by local instability and failure. The corresponding maximum stress reaches 235 MPa, which is equivalent to the ultimate strength of the selected steel material. In practice, the steel in gypsum-filled steel tubes (GCTSP) near the loading point reaches its ultimate stress of 235 MPa before the ultimate load is attained. After localized failure occurs, the presence of gypsum facilitates stress redistribution in the composite beam, decreases the stress level in the steel. The ultimate load of GCTSP exceeds that of conventional steel tubes (CTSP) due to the interaction between the two materials (steel-gypsum) which maintains the overall load-bearing capacity.As a result, the GCTSP beam lose its bearing capacity due to collapse of infilled gypsum, and the ultimate stress in the steel reaches 200 MPa according to simulation results.

Simulation of the experiment further demonstrates the enhancement effect of GCTSP. Gypsum has weaker bending resistance but possesses certain compressive strength, which synergizes well with CTSP. The steel tubes provide confinement to the internal gypsum, thereby improving the overall bending capacity of the components. Fig. 13(a) to Fig. 13(c) compare the displacement-load curves of the experiment and simulation. From the figures, it can be analyzed that the error is within 10%.

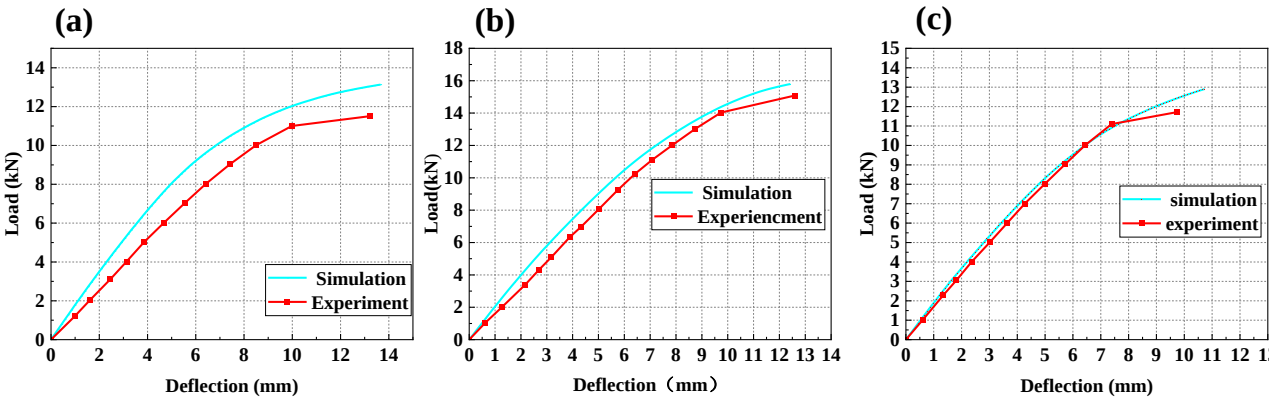

Fig. 13 Comparison between experiment and numerical simulation. (a) 80×40; (b) 80×60; (c) 80×80

4.2.2. The influence of aspect ratio

Fig. 14(a) presents the numerical simulation results for five cases with cross-sectional widths ranging from 40 to 80. The strength of each cross-section is closely related to its height-to-width ratio. This observation highlights the significant influence of the aspect ratio of the section [17]. This trend aligns with the findings in this paper on GCTSP. Specifically, the aspect ratio of 80mm×40mm is 2.0, 80mm×50mm is 1.6, 80mm×60mm is 1.33, 80mm×70mm is 1.14, and 80mm×80mm is 1.0. In Fig. 14(b), as the width decreases from 80 mm (1.0) to 50 mm (1.6), the bearing capacity gradually increases. However, when the width is reduced to 40 mm (2.0), the bearing capacity decreases. The aspect ratio exerts a pronounced constraint effect on the gypsum filling material within a specific range. In gypsum-reinforced steel tubes, the aspect ratio influences the constraint effect of the steel tube on the internal gypsum, subjecting the gypsum to three-dimensional compression and improving its compressive strength. The gypsum inside the steel tube effectively prevents local buckling, while the optimal aspect ratio enables both materials to utilize their respective properties, thereby improving the overall bending capacity of the component .

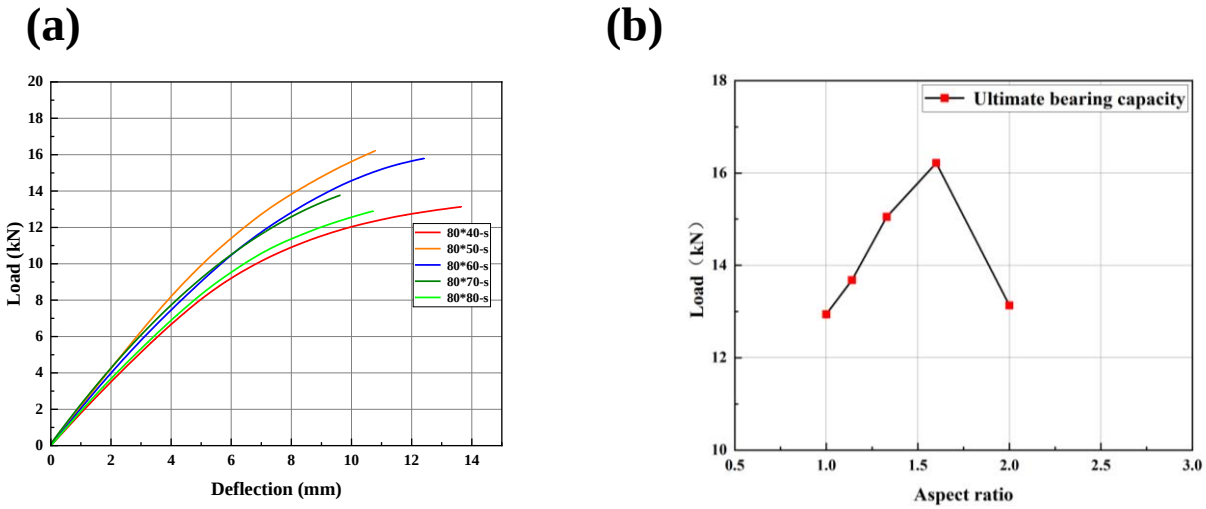

Fig. 14 (a) The ultimate bearing capacity of different size components; (b) Height-width ratio and bearing capacity curve

5. Bearing capacity calculation formula

5.1. Bending capacity calculation

Presently, composite members involving steel tube filling materials primarily focus on concrete-filled steel tubes, with theoretical calculations often considering the compressive capacity of the filled concrete. Building upon the principles of concrete-filled members, this paper incorporates considerations for the steel tube's yield capacity, local damage, gypsum compressive strength, and aspect ratio.

Han et al. [22] has proposed a semi-empirical theoretical formula for calculating the ultimate bending bending capacity of the CSTS, as shown in Eq.3.

$$M_u = \gamma_m W_s f_y, \tag{3}$$

where W_s is the sectional bending modulus, γ_m is the calculation coefficient, and f_y is the axial compression yield limit $\gamma_m = -0.2428\xi + 1.4103\sqrt{\xi}$, $\xi = (f_y A_s)/(f_{ck} A_c)$ is the constraint effect coefficient, A_s and A_s are the cross-sectional area of steel tube and concrete respectively, f_{ck} is the standard value of concrete compressive strength. Further, Li Liming et al. [23,24] introduced the plastic development coefficient of steel on the basis of considering the constraint effect.

$$M_u = (1 + \alpha) W_s f_y, \tag{4}$$

where $\alpha = A_s/A_c$ is the steel ratio of concrete filled steel tube section, (1+α) is the plastic development coefficient of steel.

Due to the calculation theories of Eq.3 and Eq.4 both designed for concrete-filled steel tubes, significant discrepancies are observed when applied to GCTSP. The errors in the calculations by Eq.3 range from a minimum of 100% to a maximum of 338%, while those by Eq.4 exhibit errors ranging from 158% to 432%. These results highlight the incompatibility of concrete-filled steel tube theories with GCTSP calculations, necessitating the introduction of new coefficients and theories for more accurate optimization.

As concrete and gypsum are both cementitious materials, they have similar characteristics in some mechanical properties. However, concrete has higher compressive strength and forms a stronger bond with CTSP. In contrast, the bond between gypsum and CTSP is weaker compared to concrete. Therefore, the constraint effect of the steel tube will be weakened, and the plastic development of the steel tube and the influence of the aspect ratio should also be considered. The following assumptions are made for GCTSP: (i) Considering the influence of aspect ratio β.(ii) Considering the constraint effect and the plastic development of steel, the correction is made by using β.

Under the above assumptions, formulas (5) and (6) are proposed to calculate the bending capacity of GCTSP.

$$M = \xi \beta W_s f_y, \tag{5}$$

$$\beta = 2.15x - 0.68x^2 - 1.2, \tag{6}$$

in the formula: M for the bending bearing capacity of the component; W_s is the section bending modulus of the rectangular steel tube; f_y for the yield strength of the steel material; β is the plastic development coefficient of steel considering the influence of aspect ratio; x is aspect ratio. $\xi = (f_y A_s)/(f_{gk} A_g)$, A_s and A_g are the cross-sectional area of steel tube and gypsum respectively, f_{gk} indicates is the standard value of gypsum compressive strength.

The analysis of the aspect ratio's influence on bending capacity reveals a direct relationship between the aspect ratio and the ultimate bending capacity. Additionally, when inversely calculating the plastic development coefficient, the obtained value of " β " aligns with the trend of the bearing capacity. Therefore, the plastic development coefficient is determined through curve fitting. The fitting curve is illustrated in Fig. 15. Utilizing the formulas (5) and (6), the corresponding findings are provided in Table 5.

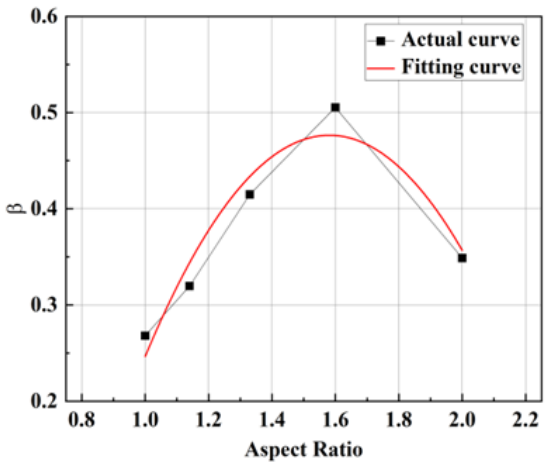

Fig. 15 Fitting curve of aspect ratio and coefficient β

Table 5
Theory and experimental results

Number	Specimens Number	M_u/kN	M_{u2}/kN	$\lvert M_u - M_{u2} \rvert / M_u$
1	80×40-s	11.5	11.1	3%
2	80×50-s	16.0	16.6	4%
3	80×60-s	15.1	15.4	2%
4	80×70-s	12.8	12.3	4%
5	80×80-s	11.4	11.3	1%

From the calculated results and experimental results, it can be observed that they are in good agreement, with an error of approximately 4%. The reason for the lower theoretical value is that it does not consider the enhanced effect of the lateral confinement of the steel tube during the actual loading process. Although this semi-empirical formula has certain practical value, its accuracy and scope of application have certain limitations, so careful evaluation and proper correction are needed in practical engineering.

6. Conclusion

This study comprehensively investigated the bending capacity of GCTSP through a combination of experimental, numerical simulation, and theoretical analyses. The key findings are summarized as follows:

- Flexural Behavior of Hollow Steel Tubes: Four-point bending experiments were performed on CTSP with 3 different cross-sectional dimensions (80mm×40mm, 80mm×60mm, 80mm×80mm). The results indicated that these tubes experienced local compression failure or warping at the loading point, leading to an ultimate flexural bearing capacity of 9.5kN, 11.5kN, and 6.9kN, respectively.
- Effect of Gypsum Infusion on Bending Capacity: Four-point bending tests were performed on GCTSP with the same three different section sizes after filling them with building gypsum. Gypsum filling effectively delayed local failure and significantly enhanced the ultimate bending capacity, resulting in capacities of 11.5kN, 15.1kN, and 11.4kN for the respective cross-sections. Compared to hollow tubes, the ultimate bending capacity increased by 22%, 36%, and 90%.
- Aspect Ratio Influence on Gypsum Effect: The effect of gypsum on flexural capacity was found to be related to the aspect ratio of the beam section. The aspect ratios of the tested sections were 2.0, 1.33, and 1, respectively, and additional aspect ratios of 1.6 and 1.14 were considered. The study revealed that, with a constant height of the steel tube (80mm), the flexural bearing capacity gradually increased with the aspect ratio. It reached a maximum at an aspect ratio of 1.6 and then decreased when the aspect ratio was reduced to 2.0. This is attributed to the dimensions of the height-to-width ratio enhancing the gypsum's constraining ability, thereby achieving the optimal coordination between the two materials.
- Numerical Simulation Validity: A 3D numerical model for the four-point bending test was created using Abaqus. Numerical simulation results closely matched experimental findings, with an agreement of about 10%.
- Semi-Empirical Formula and Correction Factor: A semi-empirical formula was developed for calculating the maximum bending capacity of GCTSP. A new correction factor (β) was introduced to consider the influence of the aspect ratio on the constraint effect. The proposed formulas demonstrated good reliability, with errors between theoretical and experimental results for ultimate load below 4%.

Overall, the study offers valuable insights into the flexural behavior of GCTSP, providing a thorough understanding through experimental, numerical, and theoretical methods.

Credit authorship contribution statement

Bo Su: Conceptualization, Methodology, Formal analysis, Writing – original draft, Writing – Review & Editing; **Yiwen Liu:** Formal analysis, Visualization, Writing – original draft, Writing – Review & Editing; **Jiao Zhang**: Writing - review & editing Investigation Validation.

Declaration of competing interest

The authors declare that they have no known competing financial interests or personal relationships that could have appeared to influence the work reported in this paper.

Acknowledgments

The research in this paper was supported by three foundations: (i) National Natural Science Foundation of China (grant number 51108210), (ii) Youth support foundation of Jiangsu University (grant number 5621480001), (iii) Zhenjiang Key Research and Development Project (Grant No. GY2021006).

Reference

[1] H. Dong, Y. Jin, W. Cao, X. Liang, S. Liu, Seismic performance of wooden straight-tenon joints reinforced with lightweight steel members, Engineering Structures. 282 (2023) 115825.
[2] Z. Fırat Alemdar, F. Alemdar, Progressive collapse of a steel structure under expected snow loads, Engineering Failure Analysis. 125 (2021) 105378.
[3] H. Peng, S. Song, H. Liu, S. Dai, F. Zhang, Investigation of wind loading characteristics of roof-mounted solar panels on tall buildings, Sustainable Energy Technologies and Assessments. 54 (2022) 102800.
[4] C. Tao Y. Zheng, Deng B. "Study on Seismic Behavior of Double Leg C-Type Cold-Formed Thin-Walled Steel Frame." Journal of Constructional Steel Research, vol. 209, Oct. 2023, p. 108035.
[5] 'Sudden! A viaduct under construction collapsed, and a car was hit and buried. _ Accident _ Fujian _ case. ' www.sohu.com/a/587887907_162758. Accessed 21 July 2023.
[6] 'Typhoon area photovoltaic bracket ' flip belly ' Gust coefficient and wind vibration coefficient of 1.0? Big mistake! 'Kandra, 12 Aug. 2019,_www.cd-class.com/a369e594f6/. Accessed 21 July 2023.
[7] Y Shao, L Peng. Finite element analysis of local buckling instability of thin-walled square steel tubes under axial compression. Journal of Yantai University (Natural Science and Engineering Edition). Apr. 2008, 304-309.
[8] P. Pannuzzo, C Ming, Flexural behaviour of cold-formed steel square and rectangular hollow sections with moderate heat-treatment, 197 (2022) 107454–107454.
[9] Eurocode 4: Design of Composite Steel and Concrete Structures[S]. Part 2: Bridge ENV, 1994-2,2001.
[10] American Institute of Steel Construction. Steel Construction Manual. American Institute of Steel Construction, 2015.
[11] M. Bosco, E. Mangiameli, P.P. Rossi, Influence of uncertainties on the seismic performance of steel moment resisting frames, Journal of Constructional Steel Research. 205 (2023) 107811.
[12] L. Xiao. "Research progress of steel-concrete composite bridge in 2019." Journal of Civil and Environmental Engineering 42 (2020) 168-182.
[13] Z. Chen, H. Ban, and Y. Wang. Research progress on the application of high-capacity steel in concrete-filled steel tubular structures. Collection of papers of the 17th (ISSF-2021) Academic Exchange and Teaching Seminar of Structural Stability and Fatigue Branch of China Steel Structure Association.
[14] S. Wu, W. Liu, J. Zhang, W. He, Y. Guo, Experimental and analytical investigation of square-shaped concrete-filled steel tube columns, Journal of Constructional Steel Research. 201 (2023) 107737.
[15] Y. Xu. Experimental study on axial compression capacity of thin-walled square steel tubular short columns filled with phosphogypsum. Steel structure 38 (2023) 21-28.
[16] Y. Lv. Experimental study on axial compression capacity of circular steel tube-gypsum-waste concrete block composite columns. New building materials 46 (2019) 19-21.
[17] L. Guo, and S. Zhang. The effect of section length-width ratio on the mechanical properties of high strength concrete filled rectangular steel tube. Journal of Harbin Institute of Technology. 2007: 530-535.
[18] Standard Test Method for Flexural Strength of Concrete (Using Simple Beam with Third-Point Loading): [C78/C78M-21]
[19] Y. Cao, and Y. Yin. Research on practical analysis method of concrete dense column gypsum composite wallboard. Proceedings of the 12 th National Symposium on Modern Structural Engineering and the 2 nd National Symposium on Technical Exchange of Cable Structures. Ed. Industrial Architecture Journal, (2012), 1163-1167.
[20] B.W. Schafer, Cold-Formed Steel Behavior and Design: Analytical and Numerical Modeling of Elements and Members with Longitudinal Stiffeners (Ph.D. thesis), Cornell University, 1997.
[21] Jiang, Ao, et al. Experimental Investigation and Design of Thin-Walled Concrete-Filled Steel Tubes Subject to Bending.Thin-Walled Structures, 63 (2013) 44–50.
[22] L. Han, Y. Yang. Modern Concrete Filled Steel Tubular Structure Technology [M]. Beijing: China National Building Industry Press, (2004).
[23] L. Li, X. Jiang, Z. Chen. Numerical analysis and simplified calculation of flexural behavior of concrete-filled rectangular steel tube. Journal of Tianjin University. (2007) 990-994.
[24] L. Li, X. Jiang, Z. Chen et al. Comparison of Computational Theory of Concrete Filled Rectangular Steel Tubes. Proceedings of the 6th National Symposium on Modern Structural Engineering. Ed. Industrial Architecture Magazine. Industrial Architecture Magazine, (2006) 1499-1507.
[25] M.-T. Chen, T. Zhang, B. Young, Behavior of concrete-filled cold-formed steel built-up section stub columns, Thin-Walled Structures. 187 (2023) 110692.
[26] Z. Zhu, F. Hai, H Shi, C. Yang et al. Flexural Property Study of Multiaxial Fiber Reinforced Polymer Sandwich Panels with Pultruded Profile Cores, Thin-Walled Structures. 189 (2023) 110910.
[27] F. Meza, and B. Jurgen. Numerical Modelling of Cold-Formed Steel Built-up Columns. Thin-Walled Structures, 188 (2023) 110781.
[28] L. Han, Y. Yang. Modern Concrete Filled Steel Tubular Structure Technology [M]. Beijing: China Construction Industry Press, (2004)
[29] A. Bello, M. Su. An Assessment of Different Direct Strength Methods for Cold-Formed Thin-Walled Steel Beam-Columns under Compression and Major Axis Bending. Structures, 34 (2021) 4788–802.
[30] K Dubey, H. Byadgi, N. Raykar. Enhancing Bending Buckling Strength of Hollow Tubes Using Concrete Filling. Materials Today: Proceedings, 72 (2023) 636–42.
[31] H. Song, L. Zhou, Y. Huang, et al. Experimental Investigation on the Seismic Capacity of Phosphogypsum-Filled Cold-Formed Thin-Walled Steel Composite Walls. Thin-Walled Structures, 186 (2023) 110664.
[32] Z. Lai, Y. Jie, Xiaohui Liu, et al. "High-Strength Rectangular Concrete-Filled Steel Tube Long Columns: Parametric Studies and Design." Journal of Building Engineering, 75 (2023), p. 107012.
[33] X. Li, S Zhang, W Lu, et al. Axial Compressive Behavior of Steel-Tube-Confined Concrete-Filled-Steel-Tubes. Thin-Walled Structures, 181 (2022) 110138.
[34] P. Kuan, Q. Wang, Y. Shao, et al. Test on Shearing Capacity of Concrete Filled Square CFRP-Steel Tube. Ocean Engineering, 274 (2023) 114065.
[35] H. Tang, L. Hou, Z. Yuan, et al. Eccentric Compressive Behavior of Square Concrete-Filled StainlessSteel Tube (CFSST) Stub Columns. Structures, 55 (2023) 1920–35.
[36] F. Wang, W. Xie, Bo Li, et al. "Experimental Study and Design of Bond Behavior in Concrete-Filled Steel Tubes (CFST)." Engineering Structures, 268 (2022) 114750.
[37] H. Wu, S. Chao, T. Zhou, et al. Cold-Formed Steel Framing Walls with Infilled Lightweight FGD Gypsum Part I: Cyclic Loading Tests. Thin-Walled Structures, 132 (2018) 759–70.
[38] L. Zhong, L. Guo, C. Jia, et al. Axial Compression Behavior of Stub Square Concrete-Filled Steel Tubes with Regional Defect. Engineering Structures, 278 (2023) 115510.
[39] Z. Zhu, F. Hai, H. Shi, et al. Flexural Property Study of Multiaxial Fiber Reinforced Polymer Sandwich Panels with Pultruded Profile Cores. Thin-Walled Structures, 189 (2023) 110910.
[40] S. Zong, Y. Lu, W. Ma, et al. Research on Eccentric-Compressive Behaviour of Steel-Fiber-Reinforced Recycled Concrete-Filled Square Steel Tube Short Columns. Journal of Constructional Steel Research, 206 (2023) 107910